fluids

MDPI

Article

Developing Bingham Fluid Flow in the Entrance Region Between Parallel Plates

Rachid Chebbi

Department of Chemical and Biological Engineering, American University of Sharjah, Sharjah P.O. Box 26666, United Arab Emirates; rchebbi@aus.edu

Abstract

Bingham fluids, also called Bingham plastics, are used in different industries including the production of food, pharmaceuticals, household products, construction and oil and gas drilling. The behavior of Bingham fluids is viscous above a critical shear stress and rigid-body below the threshold stress value. Knowledge of the size of the entrance region has several applications including hemodynamics and microfluidics. A model for steady Bingham fluid flow in the entrance region between parallel plates is developed using the inlet-filled region concept. A boundary layer model is used to solve the fluid flow dynamics in the inlet region up to the point where the critical shear stress is reached at the edge of the boundary layer. Beyond that point, the boundary layer does not grow, while the velocity profile keeps readjusting in the filled region to asymptotically reach the fully developed flow. The results include boundary layer thickness profiles, dimensionless pressure drop, centerline velocity, friction factor and inlet and entrance region sizes as functions of the Bingham number. The results are validated against the results for the Newtonian fluid case (Bingham fluid yield stress equal to zero) and CFD results, using the finite element method, for nonzero Bingham numbers. In addition, the results are found to asymptotically reach the fully developed flow values for the general Bingham fluid flow case. The effects of the Bingham number are addressed and compared with the literature. The present model is largely analytical, requiring minor numerical tasks.

Keywords: Bingham fluid; developing flow; entrance region; laminar flow; momentum integral method; boundary layer

1. Introduction

Rheological models for non-Newtonian fluids are provided in Ref. [1]. Bingham fluids, also called Bingham plastics, include many different liquids exhibiting rigid solid behavior below a threshold shear stress. Examples include heavy suspensions, paints, greases, pastes, jellies, and food products. Applications encompass different industries including construction, oil and gas, food and household industries, and applications related to sewage sludge, slurry handling and coating. Bingham fluid applications also include the use of magnetorheological (MR) fluids characterized by the effect of external magnetic and electrical fields on rheological properties [2,3].

The Bingham fluid model [1] has been widely used to model Bingham fluid flow. A treatment for fully developed flow can be found in [1] for flow in tubes and in parallel-plate channels. Analyses of fully developed magnetohydrodynamic flow can be found in [4–6] and the references therein.

Check for updates

Academic Editor: Georgios Georgiou

Received: 21 March 2026
Revised: 23 April 2026
Accepted: 24 April 2026
Published: 29 April 2026

Copyright: © 2026 by the author. Licensee MDPI, Basel, Switzerland. This article is an open access article distributed under the terms and conditions of the Creative Commons Attribution (CC BY) license.

The developing Newtonian flow was addressed by several investigators including Bodoia and Osterle [7], Magno et al. [8], Mohanty and Das [9] and Habib [10] for the parallel-plate channel flow. Developing Bingham fluid flow in a tube was addressed by Chen et al. [11], Shah and Soto [12], Nowak and Gajdecszko [13], Vradis et al. [14] (for simultaneously developing fluid flow and heat transfer), and Poole and Chabra [15]. More recent works include the treatment of Baioumy et al. [16] using the inlet-filled region concept to solve the case of developing Bingham fluid flow in tubes. Reviews can be found in [16,17].

The analysis of developing Bingham fluid flow between parallel plates is limited in the literature. Boualit et al. [17] addressed the simultaneous hydrodynamic and thermally developing Bingham fluid flow between parallel plates at constant temperature, using Papanastasiou regularization of the Bingham fluid model [18] and a Galerkin finite element solving model [17]. The computational results are provided for relatively small Reynolds numbers for which the boundary layer method is not applicable. The most recent CFD finite element models using Papanastasiou regularization [18] provide solutions for the Bingham plastic model using a slip boundary condition at the walls in [19], and the no-slip boundary condition in [20] for a wide range for Reynolds numbers [20]. References are provided in [20] for the behavior of viscoplastic and viscoelastic fluids, and applications of entrance region size determination in hemodynamics, microfluidics and the oil industry. Two earlier integral method investigations [21,22] are reviewed and compared in [22], with viscous dissipation included in the boundary layer in [22] and not accounted for in [21], as reported in [22]. The present work is based on the inlet-filled region concept, first proposed for Newtonian fluid flow by Ishizawa for axisymmetric flow between parallel disks [23], and then extended to developing Newtonian fluid flow in tubes in [24], and in parallel plates in [9,10]. The concept was successfully extended to developing power-law fluid flow in tubes and in parallel plates by Chebbi [25], and Rehman and Chebbi [26], respectively, and to developing Bingham fluid flow in tubes by Baioumy et al. [16]. The results are compared with the Newtonian fluid flow case (Bingham fluid stress = 0), published results for nonzero Bingham numbers, and asymptotically, with the fully developed results obtained from the fully developed model in Ref. [1] for the general Bingham fluid flow case. The present model extends the previous inlet-filled region models to the case of Bingham fluid flow between parallel plates and provides extensive results including parameters characterizing the developing approximate velocity profile. The following sections present the governing equations, the solution, and the results and discussion.

2. Governing Equations

A schematic of developing Bingham fluid flow between two horizontal parallel plates is shown in Figure 1. The inlet velocity is assumed to be uniform ([17,22]) and denoted as U_0. a represents half the spacing between the plates. The model used is based on the inlet-filled region concept as discussed in the Introduction. Viscous effects are restricted within the shaded upper and lower parts, with the boundary layer thickness, δ, increasing in the inlet region to reach a fixed value, δ_b, in the filled region.

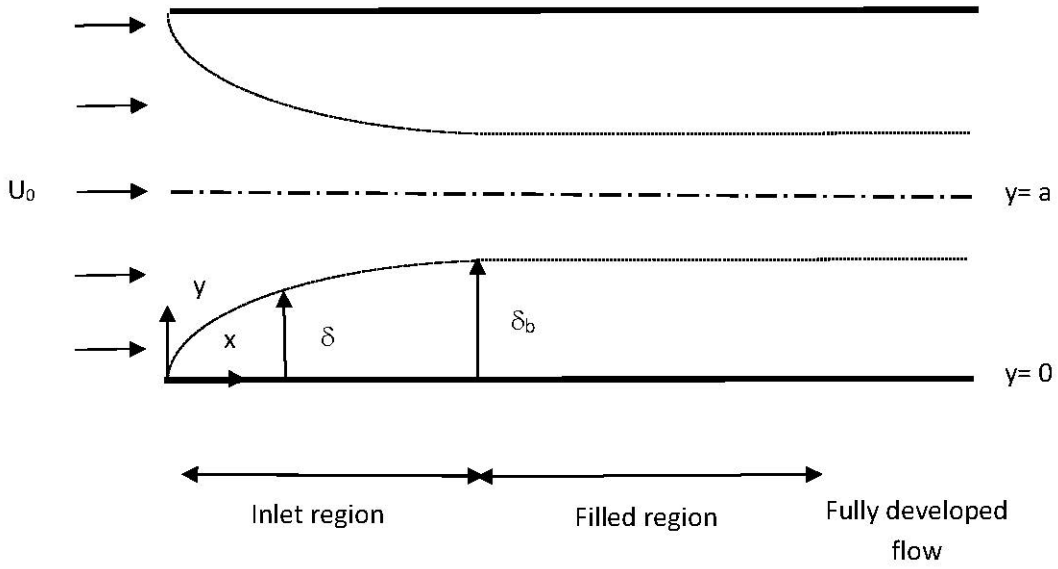


Figure 1. Schematic of Bingham fluid flow between two parallel plates, showing the inlet and filled regions forming the entrance region.

In the boundary layer zones, Bingham fluid is subject to the continuity equation

$$\frac{\partial u}{\partial x} + \frac{\partial v}{\partial y} = 0 \tag{1}$$

for constant fluid density. The velocity components u and v represent the x and y components in the axial and transverse directions, respectively. The boundary layer equations consist of the continuity equation, Equations (1) and (2) (Equation (3) in Ref. [22])

$$u\frac{\partial u}{\partial x} + v\frac{\partial u}{\partial y} = -\frac{1}{\rho}\frac{dp}{dx} + \frac{1}{\rho}\frac{\partial}{\partial y}\left[\left(\mu_0 + \tau_0\left|\frac{\partial u}{\partial y}\right|^{-1}\right)\frac{\partial u}{\partial y}\right], \tag{2}$$

where τ_0 and μ_0 denote the Bingham fluid yield stress and viscosity, respectively.

Outside the boundary layer, u is independent of y and denoted as U_∞ in the inlet region, and as U_c in the filled region.

(a) Boundary Conditions

The solution sought is an integral boundary layer method. The von Kármán method requires an approximate velocity profile in the boundary layer zone. For a quartic polynomial profile, five boundary conditions are required.

2.1. Inlet Region

The first boundary condition, (i), expresses the no-slip and no-penetration boundary conditions. The next three boundary conditions, (ii)–(iv), ensure matching between the velocity profile for u in the boundary layer and the uniform profile in the core region $u = U_\infty$

$$\text{(i) at } y = 0 \quad u = 0, v = 0 \tag{3}$$

$$\text{(ii) at } y = \delta \quad u = U_\infty \tag{4}$$

$$\text{(iii) at } y = \delta \quad \frac{\partial u}{\partial y} = 0 \tag{5}$$

$$\text{(iv) at } y = \delta \quad \frac{\partial^2 u}{\partial y^2} = 0 \tag{6}$$

In the core region, the velocity is uniform, equal to U_∞. Using Equation (2) at the interface between the boundary layer and the core region gives

$$U_\infty \frac{dU_\infty}{dx} = -\frac{1}{\rho}\frac{dp}{dx} \tag{7}$$

Using Equations (2), (3) and (7) and the definition of pressure gradient parameter λ

$$\lambda = \delta^2 \frac{\rho}{\mu_0}\frac{dU_\infty}{dx}, \tag{8}$$

gives

$$\text{(v) at y} = 0, \quad \frac{\partial^2 u}{\partial y^2} = -\frac{\lambda\, U_\infty}{\delta^2} \tag{9}$$

2.2. Filled Region

In the filled region, the boundary layer thickness remains constant and equal to the fully developed profile value, with core velocity and velocity profile in the boundary layer zone readjusting to asymptotically reach the fully developed profile.

Extending previous definitions in [16] for Bingham fluid flow in a circular tube and those in [9,10] for Newtonian fluid flow between two parallel plates, we define filled region shape factor Γ and λ as

$$\Gamma = \frac{\delta_b^2}{U_c}\left(\frac{\partial^2 u}{\partial y^2}\right)_{y=\delta_b} \tag{10}$$

$$\lambda = \delta_b^2 \frac{\rho}{\mu_0}\frac{dU_c}{dx} \tag{11}$$

The first three boundary conditions needed to determine the approximate profile are analogous to the ones mentioned earlier for the inner region:

$$\text{(i) at } y = 0 \quad u = 0, v = 0 \tag{12}$$

$$\text{(ii) at } y = \delta_b \quad u = U_c \tag{13}$$

$$\text{(iii) at } y = \delta_b \quad \frac{\partial u}{\partial y} = 0 \tag{14}$$

The fourth boundary condition is based on Equation (10)

$$\text{(iv) at } y = \delta_b \quad \frac{\partial^2 u}{\partial y^2} = \Gamma\frac{U_c}{\delta_b^2} \tag{15}$$

Applying Equation (2) at $y = \delta_b$

$$U_c\frac{dU_c}{\partial x} - \frac{\mu_0}{\rho}\left.\frac{\partial^2 u}{\partial y^2}\right|_{y=\delta_b} = -\frac{1}{\rho}\frac{dp}{dx} \tag{16}$$

and at the wall

$$\left.\frac{\mu_0}{\rho}\frac{\partial^2 u}{\partial y^2}\right|_{y=0} = \frac{1}{\rho}\frac{dp}{dx} \tag{17}$$

gives

$$\text{(v) at y} = 0 \quad \frac{U_c}{\delta_b^2}(\lambda - \Gamma) = \frac{\mu_0}{\rho}\frac{\partial^2 u}{\partial y^2} \tag{18}$$

and in dimensionless form

$$\text{at } \eta = 0, \quad \lambda - \Gamma = -\frac{\partial^2 \overline{u}}{\partial \eta^2} \tag{19}$$

(b) Integral Form of the Governing Equations

Accounting for flow symmetry, and applying the overall mass balance for a control volume extending from the inlet (x = 0) where the velocity is assumed uniform and denoted as U_0, to axial location x where the boundary layer thickness is δ and the core region velocity is U_c gives

$$2U_0 a = 2\left[\int_0^{\delta} u\, dy + U_c(a - \delta)\right] \tag{20}$$

and in dimensionless form

$$\frac{1}{\overline{U}_c} = 1 - \overline{\delta}_1 \tag{21}$$

where the dimensionless centerline velocity and displacement length are given by:

$$\overline{U}_c = \frac{U_c}{U_0}, \overline{\delta}_1 = \overline{\delta}\int_0^1 (1 - \overline{u}) d\eta \tag{22}$$

Differentiating the overall mass balance provides

$$\frac{d\overline{\delta}_1}{d\xi} = \frac{4\lambda}{\overline{\delta}^2}\frac{1}{\overline{U}_c^2} \tag{23}$$

where

$$\xi = \frac{x}{a\, Re} \quad Re = \rho U_0(4a)/\mu_0 \quad \overline{\delta} = \frac{\delta}{a} \tag{24}$$

The von Kármán integral approach is used [1]. Integration of the momentum equation between 0 and δ gives

$$\frac{d\delta_2}{dx} + (2\delta_2 + \delta_1)\frac{1}{U_c}\frac{dU_c}{dx} = \frac{\mu_0}{\rho U_c^2}\frac{\partial u}{\partial y}\bigg|_{y=0} + \frac{\delta\mu_0}{\rho U_c^2}\frac{\partial^2 u}{\partial y^2}\bigg|_{y=\delta} \tag{25}$$

Equation (25) extends Equations (2)–(46) in Ref. [10] for the Bingham fluid flow case where the boundary layer thickness δ is limited to δ_b and does not reach half the plate spacing, a. Equation (25) can be used for both inlet and filled regions, subject to the following: the second derivative to be set to zero, U_c to be replaced by U_∞ for the inlet region, and δ to be replaced by δ_b for the filled region.

$$\frac{d\overline{\delta}_2}{d\xi} = \frac{4}{\overline{\delta}\overline{U}_c}\left[\alpha + \Gamma - \frac{\lambda}{\overline{\delta}}\left(\overline{\delta}_1 + 2\overline{\delta}_2\right)\right] \tag{26}$$

where

$$\alpha = \left(\frac{\partial \overline{u}}{\partial \eta}\right)_{\eta=0}, \Gamma = \left(\frac{\partial^2 \overline{u}}{\partial \eta^2}\right)_{\eta=\overline{\delta}}, \lambda = \frac{\overline{\delta}^2}{4}\frac{d\overline{U}_c}{d\xi}, \overline{u} = \frac{u}{U_\infty}, \eta = \frac{y}{\delta} \tag{27}$$

and the dimensionless momentum thickness is defined as

$$\overline{\delta}_2 = \overline{\delta}\int_0^1 (1 - \overline{u})\overline{u}\, d\eta \tag{28}$$

subject to the following: Γ to be set to zero, $\overline{U}_c$ to be replaced by $\overline{U}_\infty$ for the inlet region, and $\overline{\delta}$ to be replaced by $\overline{\delta}_b$ for the filled region.

The pressure drop profile in the filled region is provided by Equation (16), expressed in dimensionless form as

$$\frac{d\Delta p^*}{d\xi} = \frac{8\overline{U}_c}{\overline{\delta}^2}(\lambda - \Gamma) \tag{29}$$

where the dimensionless pressure drop is defined by

$$\Delta p^* = \frac{p_0 - p}{\rho U_0^2/2} \tag{30}$$

with p_0 denoting the inlet pressure.

Integrating Equation (7) provides the following expression for the pressure drop in the inlet region

$$\Delta p = \rho \frac{U_\infty^2 - U_0^2}{2} \tag{31}$$

The friction coefficient C_f is defined as

$$C_f = \frac{2}{\rho U_0^2}\left[\tau_0 + \mu_0\left(\frac{\partial u}{\partial y}\right)_{y=0}\right] \tag{32}$$

and expressed in dimensionless form with τ_0^* representing the Bingham number, Bn

$$C_f Re = 8\left(\frac{\overline{U}_c}{\overline{\delta}}\alpha + \tau_0^*\right), \tau_0^* = \frac{a\tau_0}{\mu_0 U_0} \tag{33}$$

3. Solution

A quartic polynomial velocity profile is selected

$$\overline{u} = \sum_{k=0}^{4} a_k \eta^k \tag{34}$$

Using the above-mentioned boundary conditions gives

$$a_0 = 0, a_1 = 2 + \frac{\lambda}{6}, a_2 = -\frac{\lambda}{2} + \frac{\Gamma}{2} a_3 = -2 + \frac{\lambda}{2} - \Gamma, a_4 = 1 - \frac{\lambda}{6} + \frac{\Gamma}{2} \tag{35}$$

where Γ is zero in the inlet region. The above equations are consistent with those in [9,10] (Newtonian fluid case, Bn = 0) and found to also apply to the nonzero Bingham number, with different profiles for λ and Γ depending on Bn, as seen in the Results and Discussion.

Integrating Equations (22) and (25) yields the following expressions for the dimensionless displacement and momentum thicknesses, $\overline{\delta}_1$ and $\overline{\delta}_2$.

$$\overline{\delta}_1 = \overline{\delta}\left(1 - \sum_1^4 \frac{a_k}{k+1}\right) \tag{36}$$

$$\overline{\delta}_2 = \overline{\delta}\left(\sum_{k=1}^4 \frac{a_k}{k+1} - \sum_{k=1}^4 \sum_{j=1}^4 \frac{a_k a_j}{k+j+1}\right) \tag{37}$$

Both $\overline{\delta}_1$ and $\overline{\delta}_2$ are functions of λ in the inlet region (where Γ is zero), and Γ and λ in the filled region, as seen from the approximate profile coefficient expressions.

Using the chain rule yields the following derivatives for the unknowns $\overline{\delta}$ and λ in the inlet region

$$\begin{array}{l} \frac{d\overline{\delta}}{d\xi} = \frac{1}{D_1}\left(\frac{d\overline{\delta}_1}{d\xi}\frac{\partial\overline{\delta}_2}{\partial\lambda} - \frac{d\overline{\delta}_2}{d\xi}\frac{\partial\overline{\delta}_1}{\partial\lambda}\right), \frac{d\lambda}{d\xi} = \frac{1}{D_1}\left(\frac{d\overline{\delta}_2}{d\xi}\frac{\partial\overline{\delta}_1}{\partial\overline{\delta}} - \frac{d\overline{\delta}_1}{d\xi}\frac{\partial\overline{\delta}_2}{\partial\overline{\delta}}\right), \\ D_1 = \frac{\partial\overline{\delta}_1}{\partial\overline{\delta}}\frac{d\overline{\delta}_2}{d\lambda} - \frac{\partial\overline{\delta}_2}{\partial\overline{\delta}}\frac{d\overline{\delta}_1}{d\lambda} \end{array} \tag{38}$$

and for Γ and λ in the filled region

$$\frac{d\Gamma}{d\xi} = \frac{1}{D_2}\left(\frac{d\bar{\delta}_1}{d\xi}\frac{\partial\bar{\delta}_2}{\partial\lambda} - \frac{d\bar{\delta}_2}{d\xi}\frac{\partial\bar{\delta}_1}{\partial\lambda}\right), \frac{d\lambda}{d\xi} = \frac{1}{D_2}\left(\frac{d\bar{\delta}_2}{d\xi}\frac{\partial\bar{\delta}_1}{\partial\Gamma} - \frac{d\bar{\delta}_1}{d\xi}\frac{\partial\bar{\delta}_2}{\partial\Gamma}\right), D_2 = \frac{\partial\bar{\delta}_1}{\partial\Gamma}\frac{d\bar{\delta}_2}{d\lambda} - \frac{\partial\bar{\delta}_2}{\partial\Gamma}\frac{d\bar{\delta}_1}{d\lambda} \tag{39}$$

The inlet region is limited to zone extending from $\xi = 0$ to ξ_{in}, where $\bar{\delta}$ reaches $\bar{\delta}_b$. The limiting value determination requires consideration of the fully developed flow solution as the value of $\bar{\delta}_b$ remains uniform in the filled region.

Following [9,10,16,24], we solve for $\bar{\delta}$ and λ in the inlet region, and Γ and λ in the filled region. The determination of the profiles of $\bar{\delta}$ and λ in the inlet region, and Γ and λ in the filled region, allows calculations of the polynomial coefficients using Equation (35), the displacement and momentum thicknesses, $\bar{\delta}_1$ and $\bar{\delta}_2$, using Equations (36) and (37), and the velocity profile at any axial location using Equation (34).

(a) Fully Developed Flow

The fully developed velocity profile is symmetric and provided by [1]

$$u_{fd} = \frac{\tau_0 a}{2\mu_0}\left(\frac{a}{Y_0} - 2 - \frac{Y^2}{aY_0} + 2\frac{Y}{a}\right) \text{for } Y \geq Y_0 \tag{40}$$

$$u_{fd} = U_{c,fd} \quad \text{for } Y \leq Y_0 \tag{41}$$

where Y is the distance from the centerline, and

$$Y_0 = 1 - \delta_b \tag{42}$$

Using the fully developed profile in [1] yields in dimensionless form

$$\overline{U}_{c,fd} = \tau_0^* \frac{\bar{\delta}_b^2}{2(1-\bar{\delta}_b)} \tag{43}$$

Using the overall mass balance result in [1] and Equation (42) provides

$$\tau_0^* = 6\frac{1-\bar{\delta}_b}{\bar{\delta}_b^2(3-\bar{\delta}_b)} \tag{44}$$

and

$$\overline{U}_{c,fd} = \frac{3}{3-\bar{\delta}_b} \tag{45}$$

Using the fully developed profile and combining Equations (43)–(45) provides

$$\Gamma_{fd} = -2 \tag{46}$$

Using Equation (32) and the definition of Re in Equation (24) gives

$$C_{f,fd}Re = \frac{48}{\bar{\delta}_b^2(3-\bar{\delta}_b)} \tag{47}$$

Using Equations (28) and (45) and substituting for the limiting values $\lambda_{fd} = 0$ and $\Gamma_{fd} = -2$ (Equation (46)) yields

$$\frac{d\Delta\overline{p}_{fd}}{d\xi} = \frac{48}{\bar{\delta}_b^2(3-\bar{\delta}_b)} \tag{48}$$

Equations (29) and (33) are found to be consistent with the above equations in the fully developed flow region.

(b) Asymptotic Solution near the Inlet

Integration of the boundary layer equation is well known to present a singularity. Near the origin, the following expressions are obtained

$$\overline{\delta}_1 = \beta_1 \overline{\delta} \quad \overline{\delta}_2 = \beta_2 \overline{\delta} \tag{49}$$

where

$\beta_1 = 3/10$ and $\beta_2 = 37/315$.

Solving Equations (22) and (24) gives

$$\overline{\delta} = 4\sqrt{\frac{\xi}{\beta_2}}, \; \lambda = \frac{8\beta_1}{\beta_2}\sqrt{\frac{\xi}{\beta_2}} \tag{50}$$

The above expressions are needed to avoid the singularity at the origin.

4. Results and Discussion

The integration of Equations (38) and (39) was initiated at $\xi = 10^{-6}$ using Equations (49) and (50), and performed using the fourth-order adaptive step size Runge–Kutta FORTRAN 77 RKQC and RK4 subprograms in [27]. The profiles for boundary layer thickness vs. x/(a Re) are shown in Figure 2. The results are in very good agreement with the published works of Mohanty and Das [9] and Al-Ali [10] for the Newtonian case (Bingham number, Bn = 0).

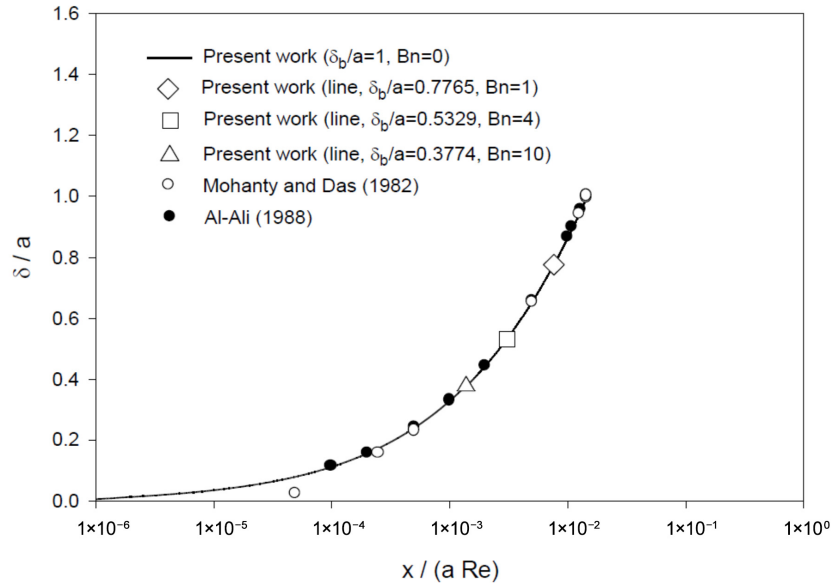


Figure 2. Profiles of dimensionless boundary layer thickness δ/a vs. x/(a *Re*) ($Re = \rho U_0(4a)/\mu_0$). Comparison with Refs. [9,10].

For Bingham numbers different from zero, the end of the inlet region is reached when the boundary layer thickness attains the fully developed value δ_b. In the filled region, the velocity profile keeps changing to asymptotically reach the fully developed profile. The maximum dimensionless thickness of the boundary layer, equal to 1 for Bn = 0, is found to decrease at higher Bn numbers and to be 0.7765, 0.5329 and 0.3774 for Bn = 1, 4 and 10, respectively.

The developing velocity profile is a function of two parameters, λ and Γ. The plots in Figures 3 and 4 show very good agreement with the results of Al-Ali [10] for Bn = 0,

with an increase in λ to a maximum at the end of the inlet region, followed by a decrease to asymptotically reach zero at the end of the filled region. The results asymptotically reach zero for λ and −2 for Γ, as expected from the fully developed profile.

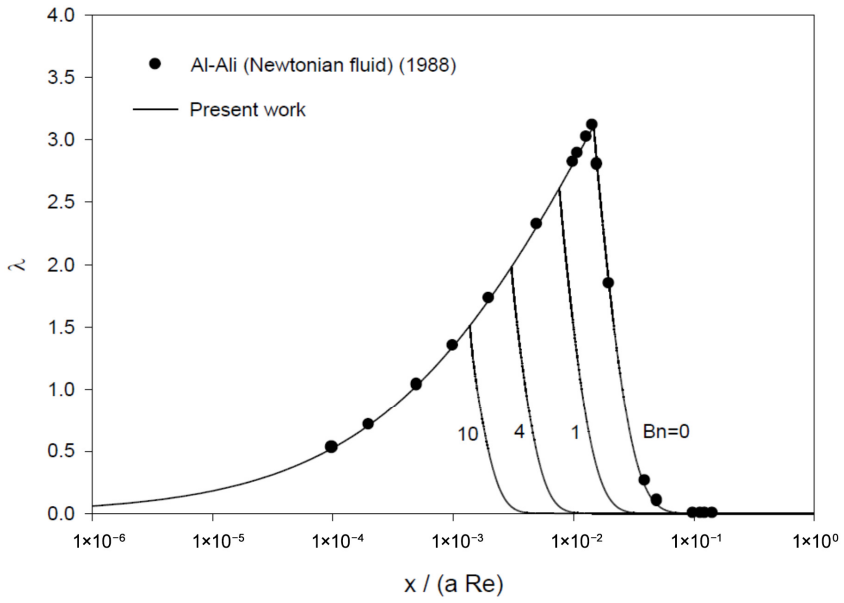


Figure 3. Profiles of pressure gradient parameter λ vs. x/(a *Re*) ($Re = \rho U_0(4a)/\mu_0$). Comparison with Ref. [10].

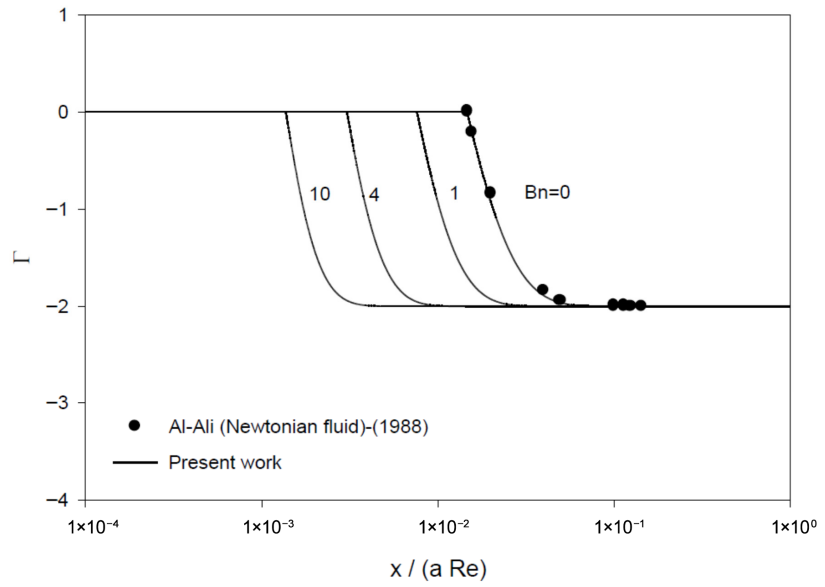


Figure 4. Profiles of filled region shape factor Γ vs. x/(a *Re*) ($Re = \rho U_0(4a)/\mu_0$). Comparison with Ref. [10].

The profiles of C_f Re (Figure 5) are in good agreement with the Newtonian fluid results of Al-Ali [10] (Bn = 0). The results show a decrease in C_f Re, at larger values of x/(a Re) and higher values of Bn, for Bn = 0, 1, 4 and 10. The asymptotically obtained values are found to match the fully developed values: 24.00, 27.80, 36.51, and 48.50 for Bn = 0, 1, 4 and 10, respectively.

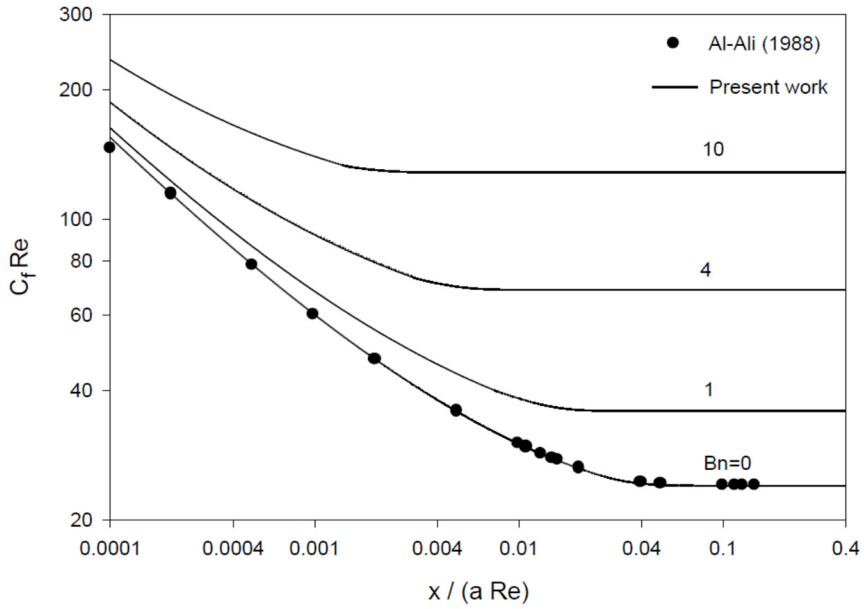


Figure 5. Profiles of C_f *Re* vs. x/(a *Re*) ($Re = \rho U_0(4a)/\mu_0$). Comparison with Ref. [10].

The plug flow velocity profiles (Figure 6) show increasing values with increasing x/a Re, and lower values of Bn. The results are validated against the Newtonian published values of Bodoia and Osterle [7], Magno et al. [8] and Al-Ali [10]. The asymptotically reached values obtained, 1.5, 1.349, 1.216 and 1.144 for Bn = 0, 1, 4 and 10, respectively, meet the fully developed values.

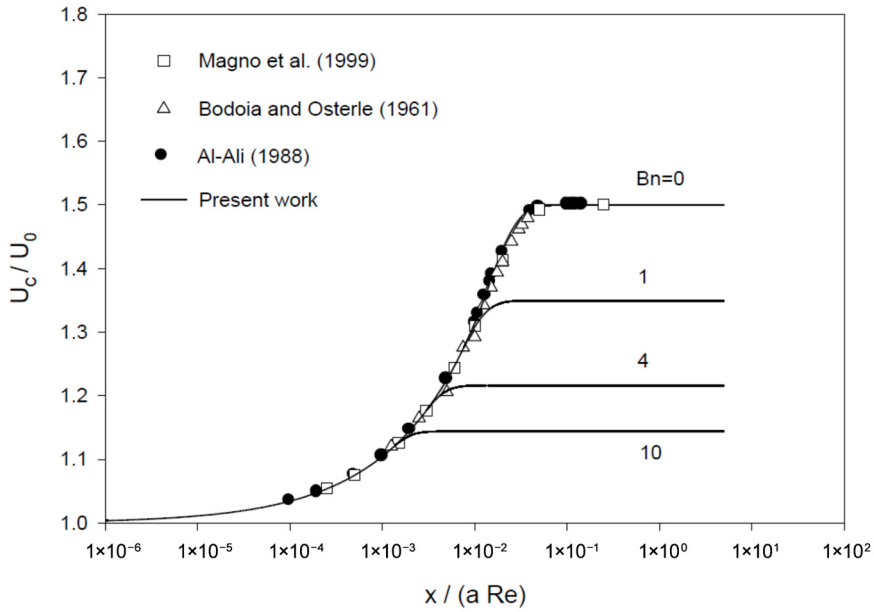


Figure 6. Profiles of dimensionless core region velocity vs. x/(a *Re*) ($Re = \rho U_0(4a)/\mu_0$). Comparison with Refs. [7,8,10].

The pressure drop profiles (Figure 7) show a very good agreement with the Newtonian fluid results, and higher pressure drop at increasing Bn.

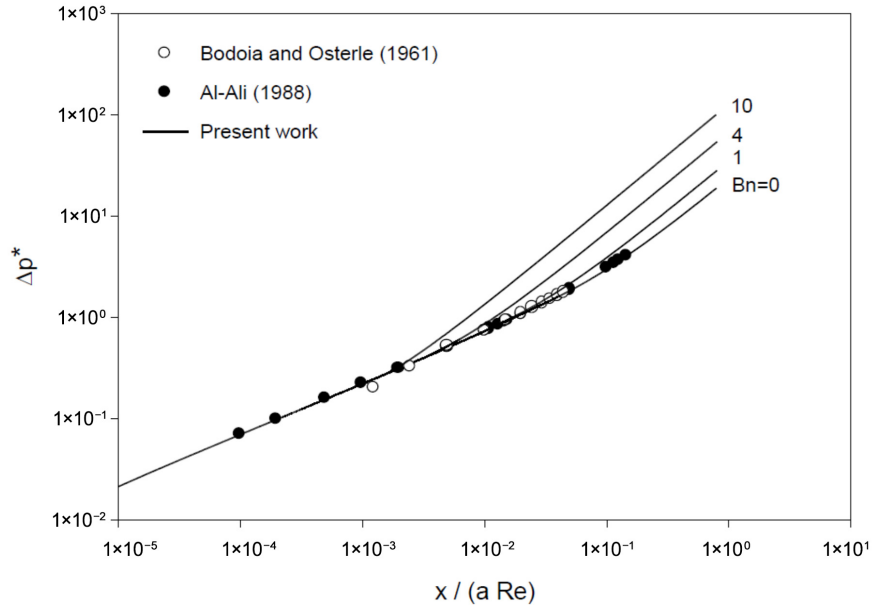


Figure 7. Profiles of Δp* vs. x/(a *Re*) ($Re = \rho U_0(4a)/\mu_0$). Comparison with Refs. [7,10].

The dimensionless inlet region lengths are found to be 0.01465, 7.603×10^{-3}, 3.043×10^{-3} and 1.372×10^{-3} for Bn = 0, 1, 4 and 10 respectively. The entrance region size is determined as the length needed to reach the fully developed value within 1%. The results are plotted vs. Bn in Figure 8, showing lower inlet and entrance region lengths at higher Bingham numbers.

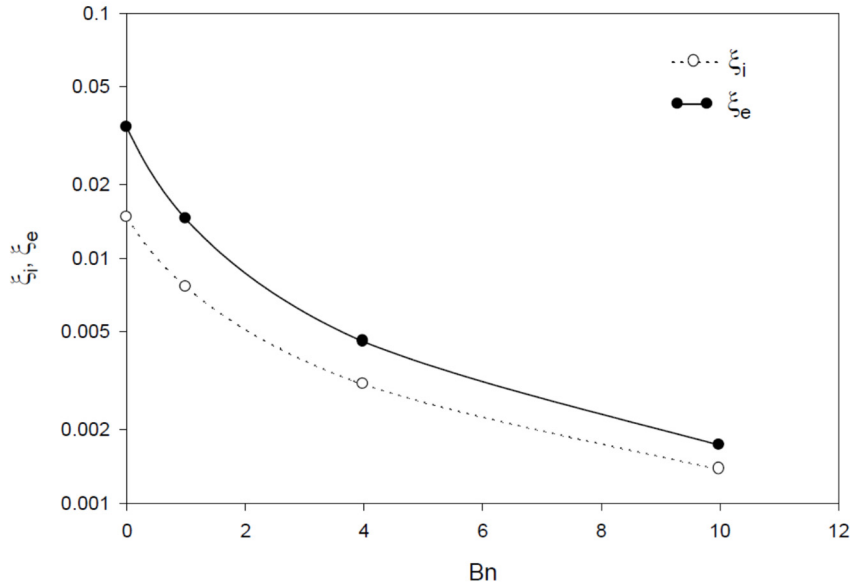


Figure 8. Profiles of dimensionless inlet region and entrance region sizes vs. Bingham number, Bn.

The entrance region length profiles are found to be in agreement with the profiles in [20] based on the same criterion: *Uc* deviating from the fully developed flow centerline velocity by 1% (Figure 9) using for comparison the definitions in [20], namely, $L_c{}^* = x_e/(2\,a) = 8\xi_e Re^*$, with Reynolds and Bingham numbers related to *Bn* and *Re* as follows: $Re^* = Re/2$ and $Bn^* = 2Bn$.

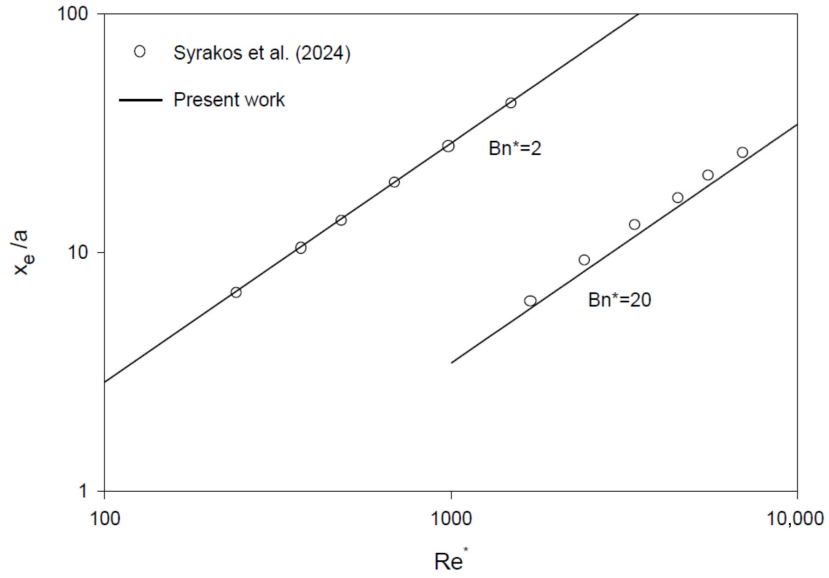


Figure 9. Compared results for the dimensionless entrance region size based on the centerline velocity criterion with Ref. [20]. (Bn* = 2 Bn, Re* = Re/2, ξ_e = 0.01438 for Bn* = 2 and 1.7248 $\times$ 10^{-3} for Bn* = 20).

Gupta's model [21] incorporates viscous dissipation in the integral mechanical energy balance and uses a quadratic approximate velocity profile expressed as a function of both the distance from the wall and the boundary layer thickness δ, with the core region velocity dependent on δ. Comparing the present results with those in [21] shows decreasing entrance region size (Figure 8 and Table 1 in [21]), and increasing pressure drop (Figure 7 and Table 2 in [21]) at higher Bn values. The trends are similar for the entrance region size in [22] (reported in Table 1 in [21]) but reversed for pressure drop (reported in Table 2 in [21]). The centerline and pressure drop profiles show consistency between the present results and those in [21] for Bn = 0.5 (Figures 10 and 11). The trends are the same for Bn = 5.0 (Figures 10 and 11), with some differences, and the fully developed solution in the present investigation asymptotically reaching the fully developed values (Figures 10 and 11). A comparison with the results in [17], obtained using a finite element model, is not possible as the boundary layer method is not applicable at relatively small Reynolds numbers, with the entrance region size tending to a limiting value, different from zero, as the Reynolds number becomes small [28].

The present model provides an analytical treatment for Bingham fluid flow in the entrance region between two parallel plates. Starting from the inlet, the size of the boundary layer thickness increases in the direction of the flow, and as a result, the size of the zone where the flow is uniform decreases. The point where the boundary layer thickness δ reaches the value of δ_b, provided by the fully developed solution, marks the end of the inlet region and the start of the filled region where the core region cross-section area remains constant and the velocity profile keeps changing to asymptotically reach the fully developed profile. The core region's velocity, U_c, is uniform in each cross-section in the filled region, but keeps changing in the direction of the flow to asymptotically reach the fully developed flow value. The size of the entrance region is defined as the location where the centerline velocity deviates by 1% from the fully developed value. Enhancement of the Bingham number, due to enhancement of the yield stress, reduces the inlet region length. The entrance region size is also found to be reduced at higher Bingham numbers in consistency with previous investigations [20,21].

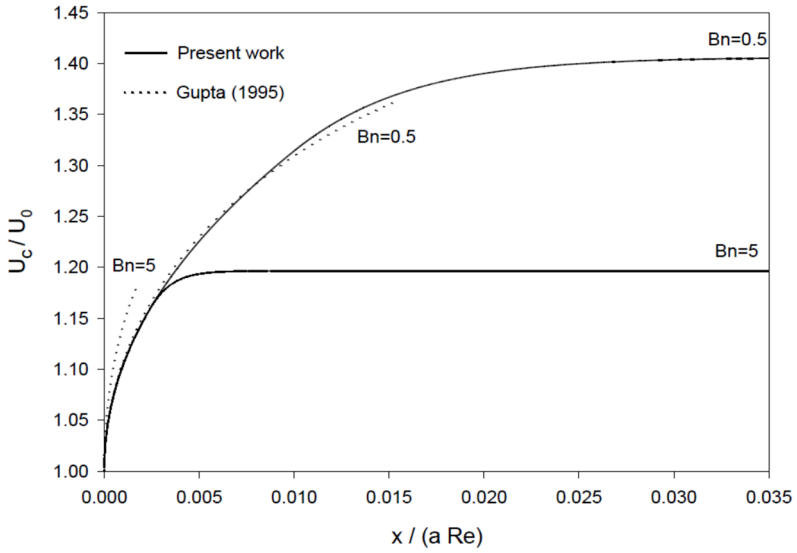


Figure 10. Comparison with centerline velocity profiles in [21] for Bn = 0.5 and 5.

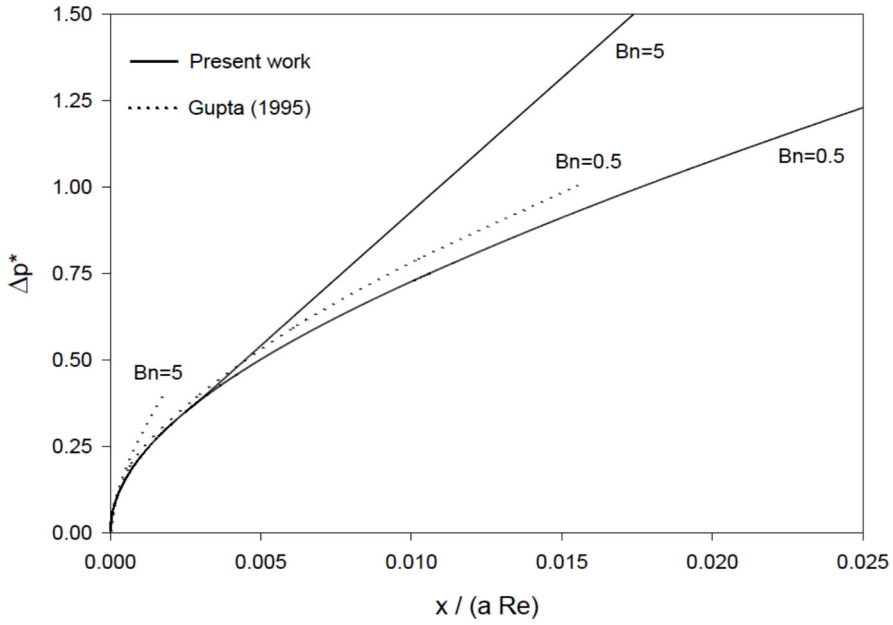


Figure 11. Comparison with pressure drop profiles in [21] for Bn = 0.5 and 5.

A quartic velocity profile is used in the present analysis. The approximate quartic velocity profile was used in a von Kármán–Pohlhausen boundary layer model [29,30] for flow past a flat plate. The accuracy of using a zero value for the second derivative as a boundary condition for the approximate velocity profile at the edge of the boundary layer in [30] was addressed in [31] in comparison with the Blasius solution [1] (providing very accurate results in comparison with experimental data [1]). The use of the quartic profile in the inlet-filled region was successful in modeling developing fluid flow in several studies including Newtonian fluid flow in circular tubes [24]. The zero second derivative boundary condition is limited to the inlet region. In the filled region, the second derivative keeps changing to asymptotically reach the fully developed value, denoted as Γ, in dimensionless form (Equation (27)). The use of the quartic profile is validated in this investigation by the good agreement with the CFD results in [20] and the asymptotic matching with the fully developed solution.

5. Conclusions

A model based on the inlet-filled region concept was developed for Bingham fluid flow in the entrance region between two parallel plates. The model extends previous inlet-filled region models. The size of the entrance region is found to decrease as the Bingham number increases. The results are new and extensive and include boundary layer thickness profiles in the inlet region, velocity profile parameters, centerline velocity, pressure drop, and friction coefficient, in addition to inlet and filled region sizes as functions of the Bingham number. The results are validated against the Newtonian fluid case (yield stress equal to zero) (Newtonian fluid case), finite element numerical results for the entrance region size based on centerline velocity criterion for Bingham numbers different from zero, and the fully developed solution for zero and nonzero Bingham numbers. Comparing the present model results with Gupta's ones shows the same trend as the Bingham number increases, with results asymptotically reaching the fully developed solution for the present model. The present model is based on boundary layer theory and is not applicable to the case of small Reynolds numbers.

Funding: This research received no external funding.

Institutional Review Board Statement: Not applicable.

Informed Consent Statement: Not applicable.

Data Availability Statement: The work is theoretical. The data used for comparison are obtained from the references mentioned in the present paper.

Conflicts of Interest: The author declares that he has no known competing financial interests or personal relationships that could have appeared to influence the work reported in this paper.

Abbreviations

a_i (i = 1–3)	coefficients in Equation (36)
Bn	Bingham number = τ_0^*
C_f	skin friction coefficient, Equation (34)
D_1, D_2	denominator terms in ODEs, Equations (40) and (41)
p	pressure, Pa
p_0	inlet pressure, Pa
Δp^*	Equation (30)
Re	Reynolds number $= \rho U_0(4a)/\mu_0$, Equation (27)
a	half of the distance between the two parallel plates, m
U_∞	plug flow velocity in the core of the cross-sectional area (inlet region), m s^{-1}
U_c	centerline velocity, m s^{-1}
$U_{c,fd}$	fully developed centerline velocity, m s^{-1}
U_0	uniform inlet velocity, m s^{-1}
$\overline{U}_\infty$	dimensionless plug flow velocity (U_∞/U_0)
$\overline{U}_c$	dimensionless centerline velocity (U_c/U_0)
$\overline{U}_{c,fd}$	dimensionless fully developed centerline velocity
u	x-component of the velocity, m s^{-1}
$\overline{u}$	dimensionless z-component of the velocity: u/U_∞ (inlet region) and u/U_c (filled region)
$\overline{u}_{fd}$	fully developed expression for u/U_c
v	y-component of the velocity, m s^{-1}
y	distance from the bottom plate, m
Y	distance from the centerline, m
Y_0	value of Y at the edge of the boundary layer (fully developed flow region), m
x	distance in the direction of the flow (u component), m

Greek Letters	
μ_0	Bingham fluid plastic viscosity, Pa s
α	dimensionless velocity gradient at the wall, Equation (29)
Γ	filled region shape factor, Equation (13)
δ	boundary layer thickness, m
$\overline{\delta}_1$	dimensionless displacement thickness, Equation (25)
$\overline{\delta}_2$	dimensionless momentum thickness, Equation (30)
$\overline{\delta}$	dimensionless boundary layer thickness, δ/a
λ	pressure gradient parameter, Equations (11) and (14)
ξ	dimensionless axial distance, $x/(Re\ a)$, Equation (27)
ξ_e	dimensionless entrance region length
ξ_i	dimensionless inlet region length
ρ	density, kg m^{-3}
τ_0	Bingham fluid yield stress
τ_0^*	dimensionless yield stress = Bn
Subscripts	
c	centerline
fd	fully developed flow
e	entrance region
f	filled region
i	inlet region
0	inlet
∞	core part in cross sectional area (inlet region)

References

1. Bird, R.B.; Stewart, W.E.; Lightfoot, E.N. *Transport Phenomena*; John Wiley & Sons: New York, NY, USA, 2007.
2. Osial, M.; Pregowska, A.; Warczak, M.; Giersi, M. Magnetorheological fluids: A concise review of composition, physicochemical properties, and models. *J. Intell. Mater. Syst. Struct.* **2023**, *34*, 1864–1884. [CrossRef]
3. Maurya, C.S.; Sarkar, C. Magnetorheological fluids: A comprehensive review of operational modes and performance under varied circumstances. *Rheol. Acta* **2024**, *63*, 765–785. [CrossRef]
4. Llorente, V.J.; Pascau, A. Numerical simulations of magnetorheological fluids flowing between two fixed parallel plates. *Appl. Math. Model.* **2019**, *74*, 151–169. [CrossRef]
5. Pourjafar, M.; Malmir, F.; Bazarganb, S.; Sadeghy, K. Magnetohydrodynamic flow of Bingham fluids in a plane channel: A theoretical study. *J. Non-Newton. Fluid Mech.* **2019**, *264*, 1–18. [CrossRef]
6. Borrelli, A.; Giantesio, G.; Patria, M.C. Exact solutions in MHD natural convection of a Bingham fluid: Fully developed flow in a vertical channel. *J. Therm. Anal. Calorim.* **2022**, *147*, 5825–5838. [CrossRef]
7. Bodoia, J.; Osterle, J.F. Finite difference analysis of plane Poiseuille and Couette flow developments. *Appl. Sci. Res.* **1961**, *10*, 265–276. [CrossRef]
8. Magno, R.; Quaresma, J.; Macedo, E. Integral transform solution for the internal boundary layer of non-Newtonian fluids. *Hybrid Methods Eng.* **1999**, *1*, 173–184. [CrossRef]
9. Mohanty, A.K.; Das, R. Laminar flow in the entrance region of a parallel plate channel. *AIChE J.* **1982**, *28*, 830–833. [CrossRef]
10. Al-Ali, H.H. Simultaneously Developing Laminar Flow and Heat Transfer in the Entrance Region of Flat and Circular Conduits. Ph.D. Thesis, Colorado School of Mines, Golden, CO, USA, 1988.
11. Chen, S.S.; Fan, L.T.; Hwang, C.L. Entrance region flow of the Bingham fluid in a circular pipe. *AIChE J.* **1970**, *16*, 293–299. [CrossRef]
12. Shah, V.L.; Soto, R.J. Entrance flow of a Bingham fluid in a tube. *Appl. Sci. Res.* **1975**, *30*, 271–278. [CrossRef]
13. Nowak, Z.; Gajdeczko, B. Laminar entrance flow of a Bingham fluid. *Acta Mech.* **1983**, *49*, 191–200. [CrossRef]
14. Vradis, G.C.; Dougher, J.; Kumar, S. Entrance pipe flow and heat transfer for a Bingham plastic. *Int. J. Heat Mass Transf.* **1993**, *36*, 543–552. [CrossRef]
15. Poole, R.J.; Chhabra, R.P. Development length requirements for fully developed laminar pipe flow of yield stress fluids. *J. Fluids Eng.* **2010**, *132*, 034501. [CrossRef]

16. Baioumy, B.; Chebbi, R.; Jabbar, N.A. Bingham fluid flow in the entrance region of a pipe. *J. Fluids Eng.* **2021**, *143*, 024503. [CrossRef]
17. Boualit, A.; Zeraibi, N.; Boualit, S.; Amoura, M. Thermal development of the laminar flow of a Bingham fluid between two plane plates with viscous dissipation. *Int. J. Therm. Sci.* **2011**, *50*, 36–43. [CrossRef]
18. Papanastasiou, T.C. Flows of materials with yield. *J. Rheol.* **1987**, *31*, 385–404. [CrossRef]
19. Philippou, M.; Kountouriotis, Z.; Georgiou, G.C. Viscoplastic flow development in tubes and channels with wall slip. *J. Non-Newton. Fluid Mech.* **2016**, *234*, 69–81. [CrossRef]
20. Syrakos, A.; Gryparis, E.; Georgiou, G.C. A revisit of the development of viscoplastic flow in pipes and channels. *J. Non-Newton. Fluid Mech.* **2024**, *334*, 105341. [CrossRef]
21. Gupta, R.C. Developing Bingham fluid flow in a channel. *Math. Comput. Model.* **1995**, *21*, 21–28. [CrossRef]
22. Batra, R.L.; Kandasamy, A. Entrance flow of Herschel-Bulkley fluids in a duct. *Fluid Dyn. Res.* **1990**, *6*, 43. [CrossRef]
23. Ishizawa, S. The axi-symmetric laminar flow in an arbitrarily shaped narrow gap: (2nd Report, theoretical analysis for the downstream region). *Bull. JSME* **1966**, *9*, 86–103. [CrossRef]
24. Mohanty, A.K.; Asthana, S.B.L. Laminar flow in the entrance region of a smooth pipe. *J. Fluid Mech.* **1979**, *90*, 433–447. [CrossRef]
25. Chebbi, R. Laminar flow of power-law fluids in the entrance region of a pipe. *Chem. Eng. Sci.* **2002**, *57*, 4435–4443. [CrossRef]
26. Rehman, S.; Chebbi, R. Power-law fluid flow in the entrance region between two parallel plates. *Results Eng.* **2024**, *24*, 103066. [CrossRef]
27. Press, W.; Flannery, B.; Teukolsky, S.; Vetterling, W. *Numerical Recipes in FORTRAN 77: The Art of Scientific Computing*, 2nd ed.; Cambridge University Press: Cambridge, UK, 1992.
28. Durst, F.; Ray, S.; Ünsal, B.; Bayoumi, O.A. The development lengths of laminar pipe and channel flows. *J. Fluids Eng.* **2005**, *127*, 1154–1160. [CrossRef]
29. von Kármán, T. Über laminare und turbulente Reibung. *J. Appl. Math. Mech.* **1921**, *1*, 233–252. [CrossRef]
30. Pohlhausen, K. Zur näherungsweisen Integration der Differentialgleichung der laminaren Grenzschicht. *J. Appl. Math. Mech.* **1921**, *1*, 252–290.
31. Majdalani, J.; Xuan, L.-J. On the Kármán momentum-integral approach and the Pohlhausen paradox. *Phys. Fluids* **2020**, *32*, 123605. [CrossRef]

Disclaimer/Publisher's Note: The statements, opinions and data contained in all publications are solely those of the individual author(s) and contributor(s) and not of MDPI and/or the editor(s). MDPI and/or the editor(s) disclaim responsibility for any injury to people or property resulting from any ideas, methods, instructions or products referred to in the content.